

# Quantum dot single photon sources with ultra-low multi-photon probability

Lukas Hanschke<sup>†,1</sup>, Kevin A. Fischer<sup>†,2</sup>, Stefan Appel,<sup>1</sup> Daniil Lukin,<sup>2</sup> Jakob Wierzbowski,<sup>1</sup> Shuo Sun,<sup>2</sup> Rahul Trivedi,<sup>2</sup> Jelena Vučković,<sup>2</sup> Jonathan J. Finley,<sup>1</sup> and Kai Müller<sup>1,\*</sup>

<sup>1</sup>*Walter Schottky Institut and Physik Department,  
Technische Universität München, 85748 Garching, Germany*

<sup>2</sup>*E. L. Ginzton Laboratory, Stanford University, Stanford, California 94305, USA*

(Dated: October 2, 2018)

High-quality sources of single photons are of paramount importance for quantum communication, sensing and metrology. To these ends, resonantly excited two-level systems based on self-assembled quantum dots have recently generated widespread interest. Nevertheless, we have recently shown that for resonantly excited two-level systems, emission of a photon during the presence of the excitation laser pulse and subsequent re-excitation results in a degradation of the obtainable single-photon purity. Here, we demonstrate that generating single photons from self-assembled quantum dots with a scheme based on two-photon excitation of the biexciton strongly suppresses the re-excitation. Specifically, the pulse-length dependence of the multi-photon error rate reveals a quadratic dependence in contrast to the linear dependence of resonantly excited two-level systems, improving the obtainable multi-photon error rate by several orders of magnitude for short pulses. We support our experiments with a new theoretical framework and simulation methodology to understand few-photon sources.

## INTRODUCTION

Two-level systems (2LS) provided by excitonic transitions in self-assembled quantum dots (QDs) are commonly used on-demand sources for high-quality single photons [1, 2]. Crucially, resonant excitation enables nearly transform-limited linewidth [3–5] and high photon indistinguishability [6]. Combined with nanoresonators, single-photon sources with high emission rates and collection efficiency have been demonstrated [7–14] and are now being incorporated into quantum information processors. For example, a solitary high-quality QD source was recently used in exciting demonstrations to create a train of single photons, which were temporally multiplexed to the input of a Boson Sampler [15, 16]. Boson sampling with this source, to date, has provided one of the best experimental validations of optical quantum computing. The quality of the experimental data in this, and future optical quantum information processors, ultimately relies on the ability of the source to emit precisely one photon when triggered by a laser pulse. However, it has recently been shown (from our work [17–19] and others [20]) that resonant excitation of a 2LS provides a fundamental limitation to the error rate of the single-photon source and hence the information processor. This results from the emission of a photon during the presence of the excitation pulse which leads to re-excitation and multi-photon emission.

In this letter, we investigate an alternative scheme which is based on a four-level system, given by the

biexciton-exciton ladder in a QD, and demonstrate that it facilitates significantly higher single-photon purity than a resonantly driven 2LS due to dramatically reduced re-excitation. At the same time, it maintains a simple implementation and high single-photon generation rates. Moreover, it enables an even higher brightness since it eliminates the need for polarization suppression of the excitation laser.

## RESULTS

We first provide detailed experimental results supporting that the bi-excitonic system is a superior single-photon source over a two-level system due to re-excitation. Second, we provide a new theoretical analysis for photon sources, using the biexcitonic system as an example.

### Experimental results

The sample consists of InGaAs QDs of low areal density ( $< 1\mu\text{m}^{-2}$ ) embedded in the intrinsic region of an n-i Schottky diode. The QDs are grown at a distance of 35nm from the n-doped region which allows control of the charge occupancy of the QDs. A field-dependent photoluminescence measurement is presented in Fig. 1a and confirms clear charge stability plateaus for the neutral exciton transitions  $X$  and emission from a negatively charged trion ( $X^-$ ). The latter can be used as a true two-level system with emission rate  $\gamma_{X^-}$  (Fig. 1b—left) while the former is part of a four-level system given by the biexciton  $2X$ , exciton  $X$  and ground state  $0$  (Fig. 1b—right).

<sup>†</sup> These authors contributed equally.

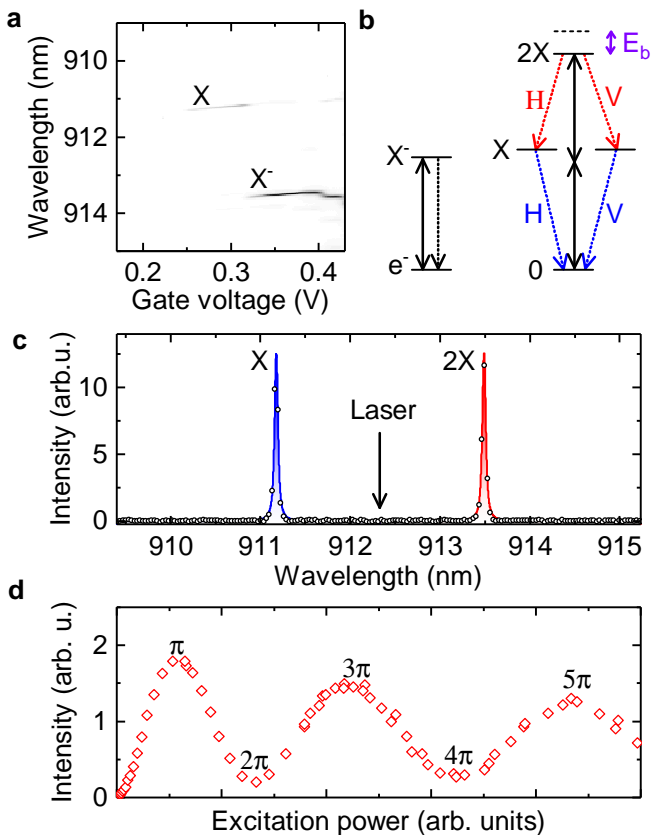


FIG. 1. **Two-photon excitation scheme.** (a) Gate voltage dependent photoluminescence. (b) Schematic illustration of resonant excitation of a 2LS and two-photon excitation of 2X. Solid arrows represent laser drive, while dotted arrows represent spontaneous emission. (c) Example spectrum for two-photon excitation of 2X at 912.34 nm. (d) Rabi oscillations between  $|0\rangle$  and  $|2X\rangle$ , measured from 2X luminescence.

Due to anisotropy in QD shape, the exchange interaction results in two  $X$  levels where one couples 2X and 0 with horizontal polarization and the other with vertical polarization [21, 22]. Depending on the specific type of QD, the two  $X$  levels are non-degenerate with a fine structure splitting of 0–100  $\mu\text{eV}$ . This system is well-known for the generation of entangled photon pairs [23–25]. Due to the Coulomb interaction, the energy of 2X is detuned from twice the  $X$  energy by the binding energy  $E_b$ . Therefore, 2X can be excited via a two-photon process where the laser energy is detuned from  $X$  by  $E_b/2$  [24, 26]. The emission rates of this system are  $\gamma_{2X}$  and  $\gamma_X$ . A typical spectrum for two-photon excitation of 2X is presented in Fig. 1c and confirms identical intensities for 2X and  $X$  emission as expected. The dependence of the emission intensity on the excitation power is presented in Fig. 1d for exciting with 3 ps long pulses and reveals clean Rabi oscillations. Time-resolved measurements reveal lifetimes of 260 ps for the emission from  $X$  and 173 ps for the emission from 2X.

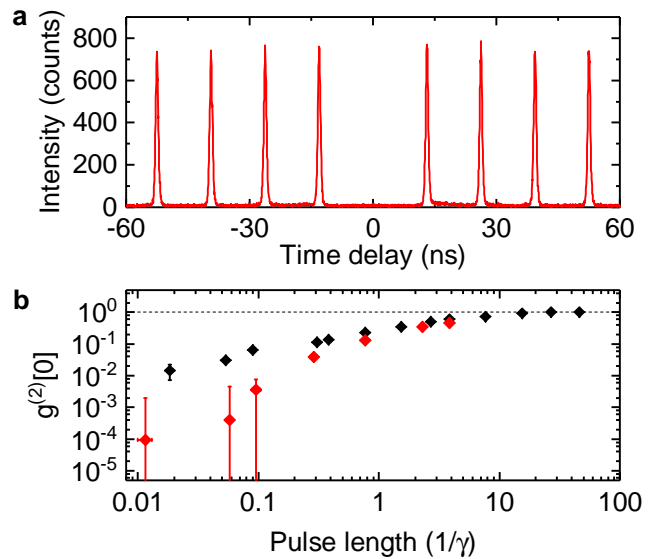


FIG. 2. **Measured degree of second-order coherence.** (a) Example of a measurement for two-photon excitation and filtering on the 2X emission using a pulse length of 3 ps. (b) Measured values of  $g^{(2)}[0]$  as a function of the pulse length for a resonantly driven two-level system (black) and two-photon excitation of 2X (red). Dashed line represents Poissonian statistics of driving laser.

To generate single photons from this system, the emission has simply to be frequency filtered to the 2X or  $X$  transition. The single-photon purity is quantified by the measured degree of second-order coherence  $g^{(2)}[0] = \langle n(n-1) \rangle / \langle n \rangle^2$  where  $n$  is the number of photons per pulse. We performed measurements of  $g^{(2)}[0]$  for two-photon excitation and frequency filtered detection on 2X using a standard HBT setup. An example measurement for 3 ps long excitation pulses of area  $\pi$  is presented in Fig. 2a. The obtained values for  $g^{(2)}[0]$  are so low that fitting the data with a series of peaks does not yield a value. Therefore, we integrate the data over an interval that contains the complete peaks (2.6 ns) and compare the integrated counts around zero time delay to the average intensity of the peaks away from zero delay. After subtracting a constant dark count background we obtain a value of  $g^{(2)}[0] = 9.4 \cdot 10^{-5} \pm 1.9 \cdot 10^{-3}$ .

The measured value of  $g^{(2)}[0]$  is lower than values obtained for a resonantly driven 2LS [17]. While the upper limit is dominated by the error which results from the dark counts of the avalanche photodiodes used here, very recently Schweickert et al have reported a value of  $g^{(2)}[0] = (7.5 \pm 1.6) \cdot 10^{-5}$  using the same scheme but superconducting detectors with negligible dark count rates [27]. As discussed above, for the resonantly excited 2LS,  $g^{(2)}[0]$  is limited by re-excitation that is enabled by emission of a photon during the presence of the pulse. In contrast, for a two-photon excitation of 2X, re-excitation is strongly suppressed. Because the laser is far detuned

from the  $2X$  transition by  $E_b/2$  re-excitation following the excitation of  $2X$  can only occur after the cascade  $|2X\rangle \rightarrow |X\rangle \rightarrow |0\rangle$  has returned the system to the ground state.

Since the re-excitation probability depends on the pulse length  $T$ , we performed measurements of  $g^{(2)}[0]$  for different values of  $T$ . The results are presented as red datapoints in Fig. 2b. For comparison, the values obtained for a resonantly driven 2LS formed by the  $X^-$  transition of the same QD are presented in Fig. 2b as black datapoints (reproduced from Ref. [19]). Thereby, the pulse lengths are normalized to  $\gamma_{X^-}$  and  $\gamma_X$ , respectively. Note, for the 2LS data and very short pulses,  $g^{(2)}[0]$  was corrected for an imperfect suppression of the excitation laser which can be quantified by electrically detuning the  $X^-$  transition [19]. For both cases  $g^{(2)}[0]$  increases with pulse length and asymptotically approaches the classical limit of 1 for long pulses. Crucially, for all measured pulse lengths, the values obtained from the two-photon excitation scheme are significantly lower than the resonantly excited 2LS. The improvement in  $g^{(2)}[0]$  amounts to an improvement of several orders of magnitude for sufficiently short pulses. A power law fit in the short pulse regime (not shown) results coefficients of  $0.73 \pm 0.07$  for the resonantly driven 2LS and  $1.89 \pm 0.40$  for the two-photon excitation scheme. This indicates a scaling behavior of approximately  $g^{(2)}[0] \propto T\gamma$  for the resonantly driven 2LS and  $g^{(2)}[0] \propto (T\gamma)^2$  for the two-photon excitation scheme, which will be confirmed in theoretical considerations below. Slight deviations of the experimental data from this behavior can be attributed to changes in the pulse shape when increasing the pulse length.

### Theoretical results

Next, we gain insight into the behavior through a theoretical study of the emission from an ideal 2LS and 2X system. First, consider an ideal two-level system [19, 28], with a ground state  $|e^-\rangle$  and an excited state  $|X^-\rangle$ . Suppose the system is driven by an optical pulse starting at  $t = 0$ , resonant with the  $|e^-\rangle \leftrightarrow |X^-\rangle$  transition and where the rotating wave approximation holds. As a function of the interacted pulse area

$$A_{2\text{LS}}(t) = \int_0^t dt' \mu \cdot E(t')/\hbar, \quad (1)$$

where  $E(t')$  is the envelope of the pulse's electric field and  $\mu$  the system's electric dipole moment, the system undergoes coherent oscillations between its ground  $|e^-\rangle$  and excited  $|X^-\rangle$  states. If the system is initially prepared in the ground state, as is typical in cryogenic experiments, the probability of the system being in the excited state  $P_{X^-}(A(t))$  shows Rabi oscillations that are nearly sinusoidal

$$P_{X^-}(A(t)) \approx \sin^2(A(t)/2), \quad (2)$$

for excitation by a short pulse relative to the spontaneous emission time of the 2LS. The Rabi oscillations are captured by the Hamiltonian (in a reference frame rotating at the laser frequency)

$$H_{2\text{LS}}(t) = \frac{\mu \cdot E(t)}{2} (|e^-\rangle \langle X^-| + |X^-\rangle \langle e^-|), \quad (3)$$

where  $\sigma = |e^-\rangle \langle X^-|$  is the system's dipole operator.

Second, to model the 2X system we will actually use only a three-level system (3LS) with levels labeled as  $|0\rangle$ ,  $|X'\rangle$  and  $|2X\rangle$ . Although there is strictly no transformation that makes these systems equivalent, if the polarization of photons emitted is disregarded in the photon counting procedure, then the behavior of the 3LS mirrors that of the 2X system. Since a two-photon transition excites the system  $|0\rangle \leftrightarrow |2X\rangle$  via the intermediate state  $|X'\rangle$ , the system undergoes Rabi oscillations that scale linearly with the pulse power rather than the field. Hence,

$$A_{3\text{LS}}(t) = \int_0^t dt' \frac{(\mu \cdot E(t'))^2}{\hbar E_b} \quad (4)$$

and

$$H_{3\text{LS}}(t) = \frac{(\mu \cdot E(t))^2}{2E_b} (|0\rangle \langle 2X| + |2X\rangle \langle 0|) \quad (5)$$

where  $\sigma \in \{|0\rangle \langle X'|, |X'\rangle \langle 2X|\}$  are the system's dipole operators. The operator  $|0\rangle \langle 2X|$  only appears after adiabatic elimination of the intermediate state.

The dynamics of the systems under spontaneous emission into Markovian reservoirs are captured in the density operator for the systems, whose evolutions can be written in terms of a Liouvillian as

$$\begin{aligned} \rho(t_1) &= \mathcal{V}(t_1, t_0)\rho(t_0) \\ &= T_{\leftarrow} \exp \left[ \int_{t_0}^{t_1} dt \mathcal{L}(t) \right] \rho(t_0), \end{aligned} \quad (6)$$

where  $T_{\leftarrow}$  is the chronological operator which orders the infinitesimal products in Eq. 6. The Liouvillian is a superoperator defined by

$$\mathcal{L}(t)\rho(t) = -i[H(t), \rho(t)] + \sum_k \mathcal{D}[L_k]\rho(t), \quad (7)$$

with the Dissipator defined as

$$\mathcal{D}[L]\rho(t) = \mathcal{J}[L]\rho(t) - \frac{1}{2}\{L^\dagger L, \rho(t)\} \quad (8)$$

and the recycling (or emission) superoperator

$$\mathcal{J}[L]\rho(t) = L\rho(t)L^\dagger. \quad (9)$$

Finally,  $L_k$  are the loss operators defined by the system operators  $\sigma_k$  and their coupling rates to the reservoirs  $\gamma_k$ , i.e.  $L_k = \sqrt{\gamma_k}\sigma_k$ . Even though the 2X system physically emits into the same reservoirs for  $|2X\rangle \rightarrow |X\rangle$

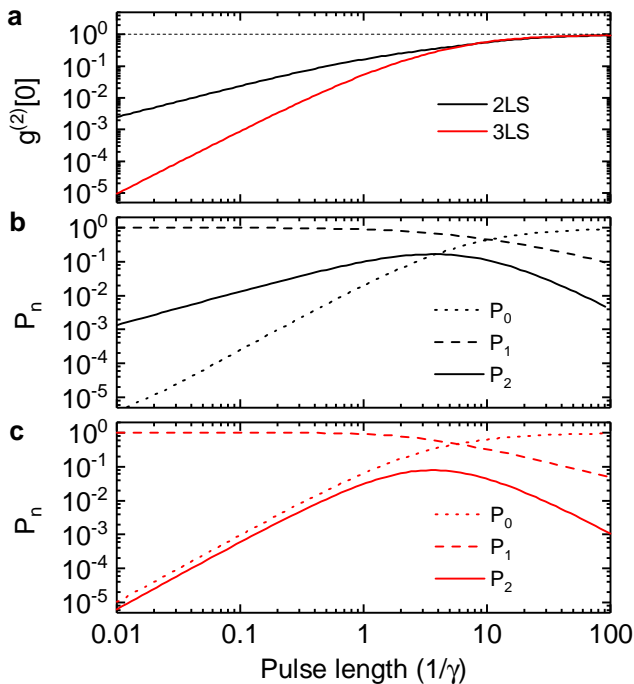


FIG. 3. **Probabilities for different photodetection events.** (a) Simulated values of  $g^{(2)}[0]$  as a function of the pulse length for a resonantly driven two-level system (black) and two-photon excitation of 2X (red). Dashed line represents Poissonian statistics of driving laser. (b-c) Simulated photocount distribution  $P_n$ , i.e. the probability for  $n$  different detections to occur, either from the emission of (b) a 2LS or (c) a 3LS filtered on either the 2X or  $X'$  transition frequency.

and  $|X\rangle \rightarrow |0\rangle$ , they are at such different frequencies ( $E_b \gg \gamma, \gamma_X, \gamma_{2X}$ ) they can be considered to emit into separate Markovian reservoirs.

We can then calculate the pulse-wise second-order coherences  $g_k^{(2)}[0]$  from the integrated versions of the correlators [17]

$$G_k^{(2)}(t_1, t_2) = \text{tr} [\mathcal{J}[L_k] \mathcal{V}(t_2, t_1) \mathcal{J}[L_k] \mathcal{V}(t_1, 0) \rho(0)]. \quad (10)$$

These coherences were calculated for  $A = \pi$  pulses (we took  $\gamma = \gamma_X = \gamma_{2X}/2$ ), driving both the 2LS (Fig. 3a—black) and 3LS (Fig. 3a—red), and they very closely match the experimental results of Fig. 2b. Small differences between experiment and theory result from experimental inaccuracies, such as the error in determining the pulse area of  $\pi$ , inaccuracies in the pulse shape, as well as drifts and fluctuations in power over the duration of the measurements [19]. We also note that we performed all quantum simulations with the Quantum Toolbox in Python (QuTiP) [29].

The final goal is to compare these results to the theoretical photocount distribution  $P_n$ , from which the photodetectors sample. The ideal 2LS emits an entirely pure photonic state into the reservoir [30], whereas the 3LS

cascade is known to emit an entangled state between the reservoirs [17, 23]. From the perspective of a single reservoir, i.e. tracing over the other reservoir, this means the state could be highly mixed and hence our previous techniques would not apply easily [17, 19, 30]. Instead, we will use the Mandel photon counting formula, as connected to the system state by Carmichael [31–33]. To do this, we first define a new superoperator

$$\mathcal{K}(t_1, t_0) = T_{\leftarrow} \exp \left[ \int_{t_0}^{t_1} dt (\mathcal{L}(t) - \mathcal{J}[L_k]) \right], \quad (11)$$

which can be thought of as an unnormalized map that evolves the density matrix conditioned on no photon emissions into the  $k$ -th reservoir. Then, the total density matrix evolution can be unraveled with respect to  $n$  emissions into the  $k$ -th reservoir as

$$\rho(t) = \sum_{n=0}^{\infty} \int_0^t dt_n \int_0^{t_n} dt_{n-1} \cdots \int_0^{t_2} dt_1 \mathcal{K}(t, t_n) \mathcal{J}[L_k] \times \mathcal{K}(t_n, t_{n-1}) \mathcal{J}[L_k] \cdots \mathcal{K}(t_2, t_1) \mathcal{J}[L_k] \mathcal{K}(t_1, 0) \rho(0). \quad (12)$$

This summation is over different numbers of photon emissions into the  $k$ -th reservoir, such that the probability density for a sequence of  $n$  emissions at times  $t_1, t_2, \dots, t_n < t$  over the interval  $[0, t]$  is given by

$$p_n(t_1, t_2, \dots, t_n; [0, t]) = \text{tr} \left[ \mathcal{K}(t, t_n) \mathcal{J}[L_k] \mathcal{K}(t_n, t_{n-1}) \mathcal{J}[L_k] \cdots \mathcal{K}(t_2, t_1) \mathcal{J}[L_k] \mathcal{K}(t_1, 0) \rho(0) \right]. \quad (13)$$

We drop the time label by taking the limit

$$p_n(t_1, t_2, \dots, t_n) \equiv \lim_{t \rightarrow \infty} p_n(t_1, t_2, \dots, t_n; [0, t]), \quad (14)$$

which corresponds to the case where the system has entirely decayed after excitation by the laser pulse. In practice, we just integrate for a few spontaneous emission lifetimes after the pulse ends. Then, the photocount distribution into the  $k$ -th channel is given by

$$P_n = \int_0^{\infty} dt_n \int_0^{t_n} dt_{n-1} \cdots \int_0^{t_2} dt_1 p_n(t_1, t_2, \dots, t_n). \quad (15)$$

Note there is only one possible way to count zero photons emitted:

$$P_0 = \lim_{t \rightarrow \infty} \text{tr} [\mathcal{K}(t, 0) \rho(0)]. \quad (16)$$

To our knowledge, this is the first use of such a model to extract photocount distributions for photon sources. For a single-photon source, driven with area  $A = \pi$ , only  $P_n$  for  $n < 3$  are significant—we calculate these

probabilities in Fig. 3 for (b) the 2LS and (c) the 3LS filtered on either transition frequency. For the single-photon sources,  $g^{(2)}[0] \approx 2P_2/(P_1 + 2P_2)^2$ , which scales linearly for the 2LS and quadratically for the 3LS with pulse length. Then, the error rate for the single-photon source is directly accessible as  $P_2 \approx g^{(2)}[0]/2$ .

## DISCUSSION

As we have shown, the bi-excitonic and effective 3-level systems are superior single-photon sources to a two-level system. We briefly provide an approximate analysis which yields strong insight into the fundamental reason behind this behavior.

Previously, we derived an analytic estimate for the two-photon error rate  $P_2$  and hence  $g^{(2)}[0]$ , for short pulses

resonantly driving a 2LS [19]. Keeping only terms to first order in  $\gamma T$ , where  $T$  is the pulse length, results for short pulses are  $P_2 \approx \frac{\gamma T}{8}$  and  $g^{(2)}[0] \approx \frac{\gamma T}{4}$ . Here, we further derive an analytic estimate for the 3LS.

For the 3LS, the only way for two emissions to occur at the  $2X$  transition frequency is through the cycle of transitions

$$|0\rangle \rightarrow |2X\rangle \rightarrow |X'\rangle \rightarrow |0\rangle \rightarrow |2X\rangle. \quad (17)$$

As in the two-level system, the first emission  $|2X\rangle \rightarrow |X'\rangle$  contributes a factor of  $\gamma_{2X} \sin(\frac{At}{2T})^2$  to the emission probability density, under the approximation of a square driving pulse. After the first emission, the system is almost exclusively in  $|X'\rangle$  so  $|X'\rangle \rightarrow |0\rangle$  contributes a factor of  $\gamma_X e^{-\gamma_X t}$ . Finally,  $|0\rangle \rightarrow |2X\rangle$  again provides another  $\gamma_{2X} \sin(\frac{At}{2T})^2$ . Hence, the two-photon emission density into the first reservoir is approximately

$$p(t_1, t_2; t'_1) \approx \begin{cases} \gamma_{2X} \sin(\frac{At_1}{2T})^2 \gamma_X e^{-\gamma_X(t'_1 - t_1)} \gamma_{2X} \sin(\frac{A(t_2 - t'_1)}{2T})^2 & \text{if } 0 < t_1 < t'_1 < t_2 < T \\ \gamma_{2X} \sin(\frac{At_1}{2T})^2 \gamma_X e^{-\gamma_X(t'_1 - t_1)} \gamma_{2X} \sin(\frac{A(T - t'_1)}{2T})^2 e^{-\gamma_{2X}(t_2 - T)} & \text{if } 0 < t_1 < t'_1 < T < t_2 \\ 0 & \text{otherwise} \end{cases} \quad (18a)$$

$$\approx \begin{cases} \gamma_{2X} \sin(\frac{At_1}{2T})^2 \gamma_X \gamma_{2X} \sin(\frac{A(t_2 - t'_1)}{2T})^2 & \text{if } 0 < t_1 < t'_1 < t_2 < T \\ \gamma_{2X} \sin(\frac{At_1}{2T})^2 \gamma_X \gamma_{2X} \sin(\frac{A(T - t'_1)}{2T})^2 e^{-\gamma_{2X}(t_2 - T)} & \text{if } 0 < t_1 < t'_1 < T < t_2 \\ 0 & \text{otherwise} \end{cases} \quad (18b)$$

where  $t'_1$  is the time of emission of the first photon at the  $X$  transition frequency. Hence, the two-photon error rate at the  $2X$  frequency is

$$P_2 = \int_0^\infty \int_0^\infty \int_0^\infty dt_1 dt'_1 dt_2 p(t_1, t_2; t'_1). \quad (19)$$

In the short pulse regime

$$\begin{aligned} P_2 &\approx \gamma_{2X}^2 \gamma_X \int_0^T \int_{t_1}^T \int_{t'_1}^T dt_1 dt'_1 dt_2 \sin(\frac{At_1}{2T})^2 \sin(\frac{A(t_2 - t'_1)}{2T})^2 \\ &\quad + \gamma_{2X} \gamma_X \int_0^T \int_{t_1}^T dt_1 dt'_1 \sin(\frac{At_1}{2T})^2 \sin(\frac{A(T - t'_1)}{2T})^2 \\ &\approx \mathcal{O}(T^4) + \mathcal{O}(T^2). \end{aligned} \quad (20)$$

Since the leading order of the second integral is lowest, and for an  $A = \pi$  pulse, the 3LS has

$$\begin{aligned} P_2 &\approx \gamma_{2X} \gamma_X \int_0^T \int_{t_1}^T dt_1 dt'_1 \sin(\frac{At_1}{2T})^2 \sin(\frac{A(T - t'_1)}{2T})^2 \\ &\approx \gamma_{2X} \gamma_X T^2 \frac{\pi^2 - 8}{8\pi^2} \end{aligned} \quad (21)$$

or  $g^{(2)}[0] \approx \gamma_{2X} \gamma_X T^2 (\pi^2 - 8)/4\pi^2$ . This quadratic scaling matches exactly with the linear region of the theoretical results in Fig. 3 and the experimentally observed results in Fig. 2.

In summary, we have quantified the re-excitation process in resonantly driven 2LS and two-photon excitation in 3LS. We have demonstrated that the 3LS, and hence the  $2X$  system, dramatically suppresses re-excitation resulting in orders of magnitude better single-photon source operation. While our experiments are a proof-of-principle with a sample structure that does not provide a high collection efficiency, the technique is directly applicable to QDs embedded in nanophotonic structures where a very efficient detection of emitted photons is possible [34–37]. Beyond superior single-photon purity, the  $2X$  scheme has the advantage over a resonantly driven 2LS that no cross-polarized suppression of the excitation laser is necessary because the driving laser and emission are far detuned such that the laser can easily be spectrally filtered out. Thus, it is easier to implement, as misalignment or optical imperfections do not pose an additional possibility for multi-photon errors. For example, very short laser pulses typically degrade cross-polarized suppression due to the increased spectral width of the laser, a wavelength sensitivity of the suppression and less efficient driving. Moreover, it does not reduce the source brightness which would be the case in a resonantly driven TLS where laser and signal are orthogonally polarized but need to couple to the same transition. To

obtain high photon indistinguishability experimentally the emission has still to be filtered to one polarization, however Purcell enhancing just one polarization with a nanoresonator would transform the four-level system to an effective three-level system with a source brightness near unity. Therefore, we expect this scheme combined with appropriate nanoresonators be an excellent candidate for a single-photon source in future quantum information processors.

## METHODS

The sample investigated is grown by molecular beam epitaxy (MBE). It consists of a layer of InGaAs quantum dots with low areal density ( $< 1\mu\text{m}^{-2}$ ), embedded within the intrinsic region of a Schottky photodiode formed from an n-doped layer below the quantum dots and a semitransparent titanium gold front contact. The distance between the doped layer and the quantum dots is 35nm, which enables control over the charge status of the dot. A weak planar microcavity with an optical thickness of one wavelength is formed from a buried 18-pair GaAs/AlAs distributive Bragg reflector (DBR) and the semitransparent top contact, which enhances the in- and out-coupling of light.

All optical measurements were performed at 4.2K in a liquid helium dipstick set-up. For excitation and detection, a microscope objective with a numerical aperture of  $NA = 0.68$  was used. Cross-polarized measurements were performed using a polarizing beam splitter. To further enhance the extinction ratio, additional thin film linear polarizers were placed in the excitation/detection pathways and a single-mode fibre was used to spatially filter the detection signal. Furthermore, a quarter-wave plate was placed between the beamsplitter and the microscope objective to correct for birefringence of the optics and the sample itself.

For Figs. 1c and 1d, a weak laser background (due to an imperfect suppression of the excitation laser) was subtracted. This linearly increasing background was directly measured through electrically tuning the quantum dot out of resonance, and typically amounted to less than 10% of the signal by  $5\pi$  pulse area.

The 3ps to 80-ps-long excitation pulses were derived from a fs-pulsed titanium sapphire laser (Coherent Mira 900) through pulse shaping. For the 3ps to 25ps long pulses, a 4f pulse shaper with a focal length of 1m and an  $1,800\text{ lmm}^{-1}$  grating was used. For the 80ps long pulses a spectrometer-like filter with a focal length of 1m and an  $1,800\text{ lmm}^{-1}$  grating was used. Longer pulses were obtained through modulating a continuous wave laser. For the modulation, a fibre-coupled and EOM-controlled lithium niobate Mach-Zehnder (MZ) interferometer with a bandwidth of 10GHz (Photline NIR-MX-LN-10) was used. Such modulators allow control of the output in-

tensity through a DC bias and a radiofrequency input. The radiofrequency pulses were generated by a 3.35GHz pulse-pattern generator (Agilent 81133A). To obtain a high extinction ratio, the temperature of the modulator was stabilized and precisely controlled (1mK) using a Peltier element, thermistor, and TEC controller. This enabled a static extinction ratio  $>45\text{db}$ .

Second-order autocorrelation measurements were performed using a Hanbury-Brown and Twiss (HBT) set-up consisting of one 50:50 beamsplitter and two single-photon avalanche diodes. The measured count rate for exciting  $2X$  with a pulse of area  $\pi$  was 9 kcps and the dark count rates of the detectors are  $251 \pm 16$  cps and  $95 \pm 10$  cps. The detected photons were correlated with a Time-Harp200 time-counting module. The time-bin width was 60 ps. The integration time for Fig. 2a was 11.05 hours and for Fig. 2b between 7.52 hours and 12.27 hours. In the pulse-wise form  $g^{(2)}[0] = \frac{N_0}{N_1}$  where  $N_0$  is the integrated area of the center peak and  $N_1$  is the average area of the side peaks. We used 16 side peaks for the averaging, which is the largest number that we can record with our correlation electronics and the used bin-width of 60ps. Note, that no long-term decay of the side peaks was observed, indicating the absence of any blinking and consistent with the fact that we use electronically stabilized devices. The error in  $N_0$  and  $N_1$  is given by  $\sqrt{N_0}$  and  $\sqrt{N_1}/4$ , where the factor of 4 results from the fact that the integrated area of 16 peaks was used to calculate  $N_1$ . The error in  $g^{(2)}[0]$  can then be calculated using quadratic propagation.

The measured correlations have a constant background that results from dark counts of the detectors. To correct for the background, we first calculate the dark counts per time bin  $n_{BG}$  by averaging a large number of bins between the peaks. The background corrected value of  $g^{(2)}[0]$  is then given by  $g_{\text{corr}}^{(2)}[0] = \frac{N_{0,\text{corr}}}{N_{1,\text{corr}}}$  where  $N_{0,\text{corr}} = N_0 - N_{BG}$  and  $N_{1,\text{corr}} = N_1 - N_{BG}$ . Note, that the error still results from  $\sqrt{N_0}$  and not  $\sqrt{N_{0,\text{corr}}}$ , highlighting the importance of detectors with low dark counts for the characterization single-photon sources with ultra-low multi photon error rates.

## DATA AVAILABILITY

The data that support the plots within this paper and other findings of this study are available from the corresponding authors upon reasonable request.

## ACKNOWLEDGEMENTS

We gratefully acknowledge financial support from the DFG via the Nanosystems Initiative Munich, the BMBF via Q.Com (Project No. 16KIS0110), BaCaTeC, the International Graduate School of Science and Engineering

(IGSSE) of TUM and the National Science Foundation (Division of Materials Research Grant No. 1503759). D.L. acknowledges support from the Fong Stanford Graduate Fellowship and the National Defense Science and Engineering Graduate Fellowship. J.W. acknowledges support from the PhD programme ExQM of the Elite Network of Bavaria. J.V. gratefully acknowledges support from the TUM Institute of Advanced Study. R.T. acknowledges support from the Kailath Stanford Graduate Fellowship. K.M. acknowledges support from the Bavarian Academy of Sciences and Humanities.

### COMPETING INTERESTS

The authors declare no competing financial and non-financial interests.

### AUTHOR CONTRIBUTIONS

L.H., S.A., J.W. and K.M. performed the experiments. K.A.F., D.L., S.S. and R.T. performed the theoretical work and modelling. J.V. and J.J.F. provided expertise. K.A.F. and K.M. conceived the idea. All authors participated in the discussion and understanding of the results. L.H. and K.A.F. contributed equally.

---

\* kai.mueller@wsi.tum.de

- [1] Peter Michler, ed., *Quantum Dots for Quantum Information Technologies* (Springer, 2017).
- [2] Pascale Senellart, Glenn Solomon, and Andrew White, “High-performance semiconductor quantum-dot single-photon sources,” *Nature Nanotechnology* **12**, 1026–1039 (2017).
- [3] Jonathan H Prechtel, Andreas V Kuhlmann, Julien Houel, Lukas Greuter, Arne Ludwig, Dirk Reuter, Andreas D Wieck, and Richard J Warburton, “Frequency-stabilized source of single photons from a solid-state qubit,” *Physical Review X* **3**, 041006 (2013).
- [4] Jack Hansom, Carsten H.H. Schulte, Clemens Matthiesen, Megan J Stanley, and Mete Atature, “Frequency stabilization of the zero-phonon line of a quantum dot via phonon-assisted active feedback,” *Applied Physics Letters* **105**, 172107 (2014).
- [5] Andreas V. Kuhlmann, Jonathan H. Prechtel, Julien Houel, Arne Ludwig, Dirk Reuter, Andreas D. Wieck, and Richard J. Warburton, “Transform-limited single photons from a single quantum dot,” *Nature Communications* **6**, 8204 (2015).
- [6] Yu-Ming He, Yu He, Yu-Jia Wei, Dian Wu, Mete Atature, Christian Schneider, Sven Höfling, Martin Kamp, Chao-Yang Lu, and Jian-Wei Pan, “On-demand semiconductor single-photon source with near-unity indistinguishability,” *Nature Nanotechnology* **8**, 213–217 (2013).
- [7] N. Somaschi, V. Giesz, L. De Santis, J. C. Loredano, M. P. Almeida, G. Hornecker, S. L. Portalupi, T. Grange, C. Antón, J. Demory, C. Gómez, I. Sagnes, N. D. Lanzillotti-Kimura, A. Lemaitre, A. Auffeves, A. G. White, L. Lanco, and P. Senellart, “Near-optimal single-photon sources in the solid state,” *Nature Photonics* **10**, 340–345 (2016).
- [8] Sebastian Unsleber, Yu-Ming He, Stefan Gerhardt, Sebastian Maier, Chao-Yang Lu, Jian-Wei Pan, Niels Gregersen, Martin Kamp, Christian Schneider, and Sven Höfling, “Highly indistinguishable on-demand resonance fluorescence photons from a deterministic quantum dot micropillar device with 74 % extraction efficiency,” *Optics Express* **24**, 8539–8546 (2016).
- [9] Xing Ding, Yu He, Z.-C. Duan, Niels Gregersen, M.-C. Chen, S. Unsleber, S. Maier, Christian Schneider, Martin Kamp, Sven Höfling, Chao-Yang Lu, and Jian-Wei Pan, “On-demand single photons with high extraction efficiency and near-unity indistinguishability from a resonantly driven quantum dot in a micropillar,” *Physical Review Letters* **116**, 020401 (2016).
- [10] Yu-Ming He, Jin Liu, Sebastian Maier, Monika Emmerling, Stefan Gerhardt, Marcelo Davanco, Kartik Srinivasan, Christian Schneider, and Sven Höfling, “Deterministic implementation of a bright, on-demand single photon source with near-unity indistinguishability via quantum dot imaging,” *Optica* **4**, 802 (2016).
- [11] Kai Müller, Kevin A. Fischer, Constantin Dory, Tomas Sarmiento, Konstantinos G. Lagoudakis, Armand Rundquist, Yousif A. Kelaita, and Jelena Vučković, “Self-homodyne-enabled generation of indistinguishable photons,” *Optica* **3**, 931 (2016).
- [12] Hui Wang, Z. C. Duan, Y. H. Li, Si Chen, J. P. Li, Y. M. He, M. C. Chen, Yu He, X. Ding, Cheng Zhi Peng, Christian Schneider, Martin Kamp, Sven Höfling, Chao Yang Lu, and Jian Wei Pan, “Near-Transform-Limited Single Photons from an Efficient Solid-State Quantum Emitter,” *Physical Review Letters* **116**, 213601 (2016).
- [13] Juan C. Loredano, Nor A. Zakaria, Niccolo Somaschi, Carlos Anton, Lorenzo de Santis, Valerian Giesz, Thomas Grange, Matthew A. Broome, Olivier Gazzano, Guillaume Coppola, Isabelle Sagnes, Aristide Lemaitre, Alexia Auffeves, Pascale Senellart, Marcelo P. Almeida, and Andrew G. White, “Scalable performance in solid-state single-photon sources,” *Optica* **3**, 433 (2016).
- [14] Jake Iles-Smith, Dara P. S. McCutcheon, Ahsan Nazir, and Jesper Mørk, “Phonon scattering inhibits simultaneous near-unity efficiency and indistinguishability in semiconductor single-photon sources,” *Nature Photonics* **11**, 521–526 (2017).
- [15] J. C. Loredano, M. A. Broome, P. Hilaire, O. Gazzano, I. Sagnes, A. Lemaitre, M. P. Almeida, P. Senellart, and A. G. White, “Boson Sampling with Single-Photon Fock States from a Bright Solid-State Source,” *Physical Review Letters* **118**, 130503 (2017).
- [16] Hui Wang, Yu He, Yu-Huai Li, Zu-En Su, Bo Li, He-Liang Huang, Xing Ding, Ming-Cheng Chen, Chang Liu, Jian Qin, Jin-Peng Li, Yu-Ming He, Christian Schneider, Martin Kamp, Cheng-Zhi Peng, Sven Höfling, Chao-Yang Lu, and Jian-Wei Pan, “High-efficiency multiphoton boson sampling,” *Nature Photonics* **11**, 361–365 (2017).
- [17] K. A. Fischer, K. Müller, K. G. Lagoudakis, and J. Vučković, “Dynamical modeling of pulsed two-photon interference,” *New Journal of Physics* **18**, 113053 (2016).

- [18] Kevin A. Fischer, Lukas Hanschke, Jakob Wierzbowski, Tobias Simmet, Constantin Dory, Jonathan J. Finley, Jelena Vučković, and Kai Müller, “Signatures of two-photon pulses from a quantum two-level system,” *Nature Physics* **13**, 649–654 (2017).
- [19] Kevin A Fischer, Lukas Hanschke, Malte Kremser, Jonathan J Finley, Kai Müller, and Jelena Vučković, “Pulsed rabi oscillations in quantum two-level systems: beyond the area theorem,” *Quantum Science and Technology* **3**, 014006 (2017).
- [20] Adetunmise C Dada, Ted S Santana, Ralph NE Malein, Antonios Koutroumanis, Yong Ma, Joanna M Zajac, Ju Y Lim, Jin D Song, and Brian D Gerardot, “Indistinguishable single photons with flexible electronic triggering,” *Optica* **3**, 493–498 (2016).
- [21] M. Bayer, G. Ortner, O. Stern, A. Kuther, A. A. Gorbunov, A. Forchel, P. Hawrylak, S. Fafard, K. Hinzer, T. L. Reinecke, S. N. Walck, J. P. Reithmaier, F. Klopff, and F. Schäfer, “Fine structure of neutral and charged excitons in self-assembled In(Ga)As/(Al)GaAs quantum dots,” *Physical Review B* **65**, 195315 (2002).
- [22] J. J. Finley, D. J. Mowbray, M. S. Skolnick, A. D. Ashmore, C. Baker, A. F. G. Monte, and M. Hopkinson, “Fine structure of charged and neutral excitons in InAs-AlGaAs quantum dots,” *Physical Review B* **66**, 153316 (2002).
- [23] N. Akopian, N. H. Lindner, E. Poem, Y. Berlatzky, J. Avron, D. Gershoni, B. D. Gerardot, and P. M. Petroff, “Entangled photon pairs from semiconductor quantum dots,” *Physical Review Letters* **96**, 130501 (2006).
- [24] M. Müller, S. Bounouar, K. D. Jöns, M. Glässl, and P. Michler, “On-demand generation of indistinguishable polarization-entangled photon pairs,” *Nature Photonics* **8**, 224–228 (2014).
- [25] Daniel Huber, Marcus Reindl, Yongheng Huo, Huiying Huang, Johannes S. Wildmann, Oliver G. Schmidt, Armando Rastelli, and Rinaldo Trotta, “Highly indistinguishable and strongly entangled photons from symmetric GaAs quantum dots,” *Nature Communications* **8**, 15506 (2017).
- [26] Per Lennart Ardel, Lukas Hanschke, Kevin A. Fischer, Kai Müller, Alexander Kleinkauf, Manuel Koller, Alexander Bechtold, Tobias Simmet, Jakob Wierzbowski, Hubert Riedl, Gerhard Abstreiter, and Jonathan J. Finley, “Dissipative preparation of the exciton and biexciton in self-assembled quantum dots on picosecond time scales,” *Physical Review B* **90**, 241404 (2014).
- [27] Lucas Schweickert, Klaus D. Jöns, Katharina D. Zeuner, Saimon Filipe Covre da Silva, Huiying Huang, Thomas Lettner, Marcus Reindl, Julien Zichi, Rinaldo Trotta, Armando Rastelli, and Val Zwiller, “On-demand generation of background-free single photons from a solid-state source,” *Applied Physics Letters* **112**, 093106 (2018).
- [28] Bruce W. Shore, *Manipulating quantum structures using laser pulses* (Cambridge University Press, Cambridge, 2011).
- [29] J.R. Johansson, P.D. Nation, and Franco Nori, “Qutip 2: A python framework for the dynamics of open quantum systems,” *Computer Physics Communications* **184**, 1234–1240 (2013).
- [30] Kevin A Fischer, Rahul Trivedi, Vinay Ramasesh, Ifan Siddiqi, and Jelena Vučković, “Scattering into one-dimensional waveguides from a coherently-driven quantum-optical system,” *Quantum* **2**, 69 (2018).
- [31] Howard Carmichael, *An open systems approach to quantum optics: lectures presented at the Université Libre de Bruxelles, October 28 to November 4, 1991*, Vol. 18 (Springer Science & Business Media, 2009).
- [32] Howard M Wiseman and Gerard J Milburn, *Quantum measurement and control* (Cambridge university press, 2009).
- [33] Crispin Gardiner and Peter Zoller, “The quantum world of ultra-cold atoms and light book ii: The physics of quantum-optical devices,” in *The Quantum World of Ultra-Cold Atoms and Light Book II: The Physics of Quantum-Optical Devices* (World Scientific, 2015) pp. 1–524.
- [34] O Gazzano, S Michaelis De Vasconcellos, C Arnold, A Nowak, E Galopin, I Sagnes, L Lanco, A Lemaître, and P Senellart, “Bright solid-state sources of indistinguishable single photons,” *Nature communications* **4**, 1425 (2013).
- [35] Julien Claudon, Joël Bleuse, Nitin S. Malik, Maela Bazin, Périne Jaffrennou, Niels Gregersen, Christophe Sauvan, Philippe Lalanne, and Jean-Michel Gérard, “A highly efficient single-photon source based on a quantum dot in a photonic nanowire,” *Nature Photonics* **4**, 174–177 (2010).
- [36] M. Gschrey, A. Thoma, P. Schnauber, M. Seifried, R. Schmidt, B. Wohlfeil, L. Kruger, J. H. Schulze, T. Heindel, S. Burger, F. Schmidt, A. Strittmatter, S. Rodt, and S. Reitzenstein, “Highly indistinguishable photons from deterministic quantum-dot microlenses utilizing three-dimensional in situ electron-beam lithography,” *Nature Communications* **6** (2015).
- [37] Luca Sapienza, Marcelo Davanco, Antonio Badolato, and Kartik Srinivasan, “Dots for bright and pure single-photon emission,” *Nature Communications* **6**, 7833 (2015).